The Microwave Rotational Spectra of 1-Bromo-2,2-Difluoroethylene and the Bromine Nuclear Quadrupole Coupling Tensor

F. Oldag and D. H. Sutter

Abteilung Chemische Physik im Institut für Physikalische Chemie
der Christian-Albrechts-Universität zu Kiel

Z. Naturforsch. **46a**, 513–526 (1991); received March 14, 1991

The first assignment of the vibronic ground state rotational spectra for $F_2C{=}CH^{79}Br$ and $F_2C{=}CH^{81}Br$ is reported. Only μ_b-type transitions could be observed. This indicates, that the C–F and C–Br bond dipole moments are almost equal despite of the large difference in the Pauling electronegativities of the two halogen atoms. The complete quadrupole Br-coupling tensors including their orientation with respect to the molecular principal inertia axes could be determined and are discussed within the Townes-Dailey model. A partial r_0-structure is proposed.

Introduction

We have initiated the present study in view of our current interest in the effects of fluorine substitution on the geometries, magnetic properties and bonding in small molecules. The rather dense microwave spectrum of $F_2C{=}CHBr$ has never been studied before. So, in this initial study, we report the assignment of the spectrum and we discuss the observed bromine nuclear quadrupole coupling. Detailed studies of the Stark effect, the rotational Zeeman effect and of the ^{13}C-isotopic species are planned for the near future.

Experimental

A sample of 1-bromo-2,2-difluoroethylene, a gas at room temperature, was obtained from Fluorochem Ltd., Old Glossop (Great Britain) and was used without further purification. A rough prediction of the spectrum was calculated from an approximate structure, guessed as a composite from the structures of $F_2C{=}CH_2$ [1] and of $H_2C{=}CHBr$ [2], see Figure 1.

From this first prediction with rotational constants $A = 10.85$ GHz, $B = 1.41$ GHz, $C = 1.25$ GHz for the ^{81}Br-species and $A = 10.85$ GHz, $B = 1.43$ GHz and $C = 1.26$ GHz for the ^{79}Br-species, near prolate top μ_a- and μ_b-type spectra were calculated. Transitions, involving levels with larger K_a-quantum numbers ($K_a =$

Reprint requests to Prof. Dr. D. H. Sutter, Institut für Physikalische Chemie, Universität Kiel, Olshausenstraße 40, W-2300 Kiel, FRG.

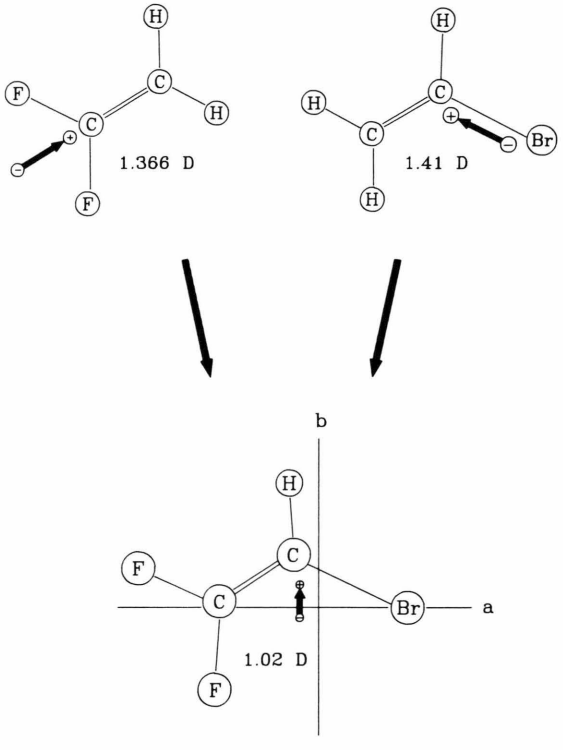

Fig. 1. Within an additivity scheme for bond moments, superposition of the electric dipole moment vectors of 1,1-difluoroethylene and bromoethylene should lead to the dipole moment of 1-bromo-2,2-difluoroethylene (the ethylene-configuration, which is additionally produced that way has zero dipole moment). Since the a-components largely compensate in such a superposition, one expects the dipole moment to be closely aligned to the *b*-axis of the moment of inertia tensor. This explains why no μ_a-type transitions and no rapid μ_a-type Stark effects could be observed.

0932-0784 / 91 / 0600-0513 $ 01.30/0. – Please order a reprint rather than making your own copy.

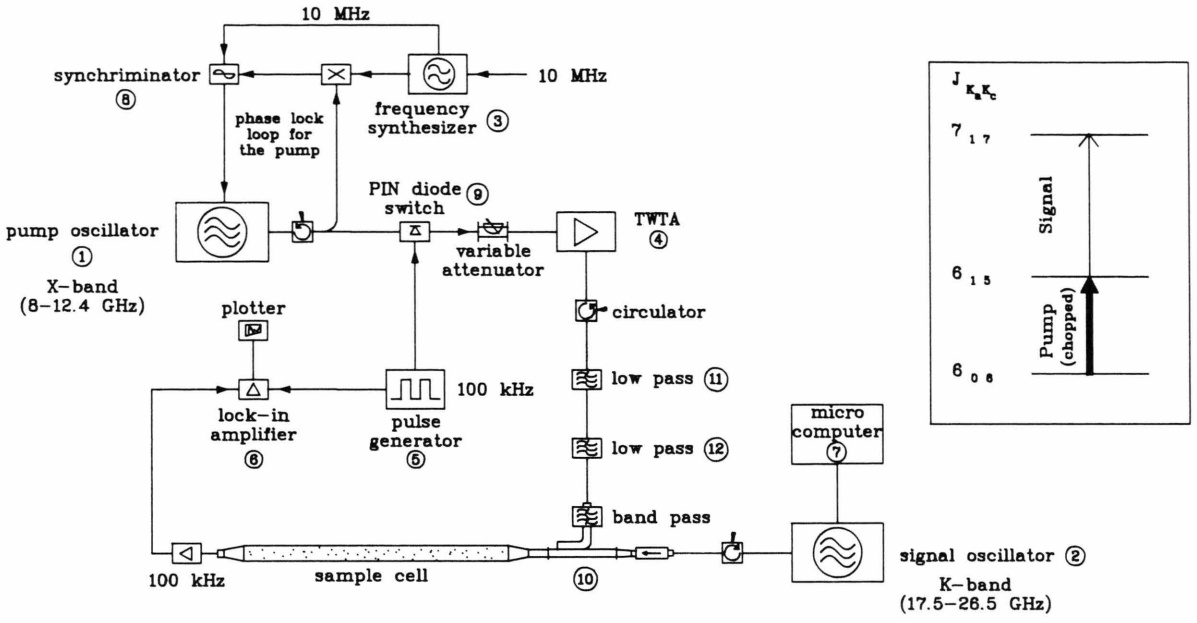

Fig. 2. Block diagram of the double resonance modulation spectrometer, which was set up to confirm the assignment of the spectra.

1) Sweeper. Hewlett Packard 8690 B with 8696 A plug in.
2) 10 MHz–26.5 GHz synthesized sweeper Hewlett Packard 8340 B.
3) Frequency synthesizer 470–1000 MHz, Rohde & Schwarz XSU, XUC.
4) X-band TWT amplifier Hughes 1177 H, 10 W.
5) Pulse generator E-H Research Laboratories 137-NV.
6) Lock-in amplifier Ithaco Dynatrac 391 A.
7) Micro computer Commodore C 64.
8) Frequency synchriminator Rohde & Schwarz XKG.
9) PIN diode switch Hewlett Packard 33144 A with TTL-driver 33190 B.
10) X-band multihole directional coupler Waveline 674-3 (3 dB) with band pass filter AEL F2001.
11) Coaxial low pass filter 15 GHz, AEL MW 1140-2.
12) Coaxial low pass filter 14 GHz, K & L Micro FLR 14.0.

K-quantum number of the limiting prolate symmetric top) were expected to exhibit rather fast Stark effects due to μ_a-matrix elements connecting the near-degenerate K_a-doublets. An extensive search with our Stark effect-modulated spectrometers [3], run at a low modulation field strength, failed to detect any such transitions. Thus, μ_a must be exceedingly small, even smaller than the value predicted from a vector addition of the reported dipole moments of $F_2C=CH_2$ [4] and $H_2C=CHBr$ [5] as also shown in Figure 1.

In a second run high-field Stark modulated spectra as well as microwave Fourier transform spectra were recorded in the X- and K-band region (8 to 26 GHz) and typical bromine quadrupole hfs patterns were searched for. Looking for the expected quadrupole hfs pattern, the $J_{0J} \rightarrow J_{1J-1}$ μ_b-type Q-branch could be tentatively assigned for both isotopic species. To confirm this tentative assignment, a microwave-microwave double resonance spectrometer was assembled as shown in Figure 2. In this spectrometer the strong X-band pump radiation is set on a tentatively assigned Q-branch transition. It is chopped (100 kHz on/off) and the signal frequency is swept over a K-band region in which a yet unassigned transition, connected to the pump transition by a three level double resonance scheme, is suspected. The insert of Fig. 2 shows an example. With lock-in detection at the modulation frequency of the pump, only those transitions which involve one of the pumped states are modulated and detected.

The correct assignment of the transitions could be easily confirmed that way, as is demonstrated in Figs. 3 and 4.

Pumping on the $7_{07} \rightarrow 7_{16}$ transition, the $7_{16} \rightarrow 7_{25}$ transition could be assigned, which gave access to the $J_{1J-1} \rightarrow J_{2J-2}$ Q-branch. Pumping on the $5_{05} \rightarrow 5_{14}$ and $6_{06} \rightarrow 6_{15}$ transitions, respectively, the $5_{05} \rightarrow 6_{16}$ and $6_{06} \rightarrow 7_{17}$ R-branch transitions could be assigned.

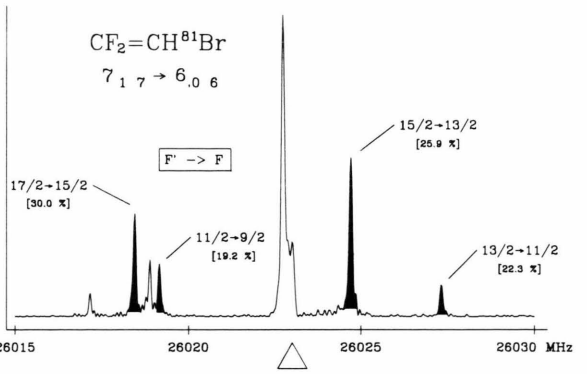

Fig. 3. 15 MHz section of a MWFT power spectrum of 1-bromo-2,2-difluoroethylene, which shows the four most intense quadrupole hfs satellites of the $7_{17} \rightarrow 6_{06}$ rotational transition of $CF_2=CH^{81}Br$. The additional four lines turned out to belong to the $7_{25} \rightarrow 7_{16}$ Q-branch transition of the same isotopic species. For the final assignment a double resonance experiment was carried out (see Figs. 2 and 4). The experimental conditions were: Sample pressure: 91 Pa (7 mTorr); temperature: −43 °C; polarization frequency: 26 023.000 MHz; delaytime after the end of the pulse: 2500 ns; sampling rate: 10 ns; 1 k data points with 3072 zeros added prior to the Fourier transformation. Relative satellite intensities of the satellites, as they would be observed in a cw-spectrometer, are given in brackets. Intensity deviations as seen here are typical for MWFT spectra. They reflect differences in the polarization efficiency due to different offsets with respect to the frequency in the polarizing pulse.

This did lead to sufficiently accurate rotational constants to identify in total 40 rotational transitions for the ^{79}Br species and 38 for the ^{81}Br species.

The spectra were analyzed using the effective Hamiltonian

$$\hat{H}_{\text{eff}}/h = \hat{H}_R/h + \hat{H}_{CD}/h + \hat{H}_Q/h \tag{1}$$

with

$$\hat{H}_R/h = A\hat{J}_a^2 + B\hat{J}_b^2 + C\hat{J}_c^2\,, \tag{1a}$$

$$\hat{H}_{CD}/h = -D_J\hat{J}^4 - D_{JK}\hat{J}^2\hat{J}_a^2 - D_K\hat{J}_a^4 - 2\delta_J\hat{J}^2(\hat{J}_b^2 - \hat{J}_c^2) - 2R_6[3\hat{J}_b^2\hat{J}_c^2 + \hat{J}_c^2\hat{J}_b^2) - \hat{J}_b^4 - \hat{J}_c^4]\,, \tag{1b}$$

$$\hat{H}_Q/h = +(1/6)\sum_i\sum_j Q_{ij}V_{ij}/h\,. \tag{1c}$$

A, B, C rotational constants;

$\hat{J}_a, \hat{J}_b, \hat{J}_c$ operators corresponding to the components of the rotational angular momentum in direction of the molecular principal inertia axes measured in units of $\hbar$;

$D_J, D_{JK}, D_K, \delta_J, R_6$ centrifugal distortion constants up to fourth order,

Q_{ij} components of the Br nuclear quadrupole moment tensor;

$-V_{ij}$ components of the intramolecular electric field gradient tensor at the position of the Br nucleus and caused by the extranuclear charge distribution.

This Hamiltonian includes the bromine nuclear quadrupole coupling, $\hat{H}_Q$, as well as centrifugal distortion corrections, $\hat{H}_{CD}$, up to fourth order. It is given in frequency units. For the derivation of the fourth order centrifugal distortion Hamiltonian we refer to [6, 7]. For a general discussion of nuclear quadrupole coupling we refer to [8].

The Hamiltonian matrix was set up in the coupled basis for the limiting symmetric top, $|J, K_a, I, F, M_F\rangle$ [9]. This matrix factorizes into F-blocks (F = quantum number corresponding to the overall angular momentum including the spin of the bromine nucleus, $\boldsymbol{I}$, and the rotational angular momentum, $\boldsymbol{J}$, but neglecting all other spins). The F-blocks were diagonalized numerically. The transition strengths were obtained by the corresponding transformation of the direction cosine matrix elements. Our program ⟨HFS⟩ [10] was used for the calculations.

Because of the small inertia defect the equilibrium configuration is clearly planar. Therefore, there are only four nonzero components of the electric field gradient tensor, caused by extra-nuclear charges, i.e. $-V_{aa}$, $-V_{bb}$, $-V_{cc}$, and $-V_{ab}$, where the diagonal elements are linearly dependent by Poisson's equation,

$$V_{aa} + V_{bb} + V_{cc} = 0\,. \tag{2}$$

Thus only

$$(\chi_{bb} + \chi_{cc}) = eQ(V_{bb} + V_{cc})/h,$$
$$(\chi_{bb} + \chi_{cc}) = eQ(V_{bb} - V_{cc})/h \quad \text{and}$$
$$\chi_{ab} = eQV_{ab}/h$$

were fitted to the observed line frequencies. Here Q stands for the so called nuclear quadrupole moment of the ^{79}Br and ^{81}Br nucleus, respectively. e stands for the proton charge, and V_{aa} etc. are the vibronic ground state expectation values for the second derivatives of that part of the intramolecular Coulomb potential which originates from charges outside the bromine nucleus.

A global fit was performed, i.e. the rotational constants, the centrifugal distortion constants and

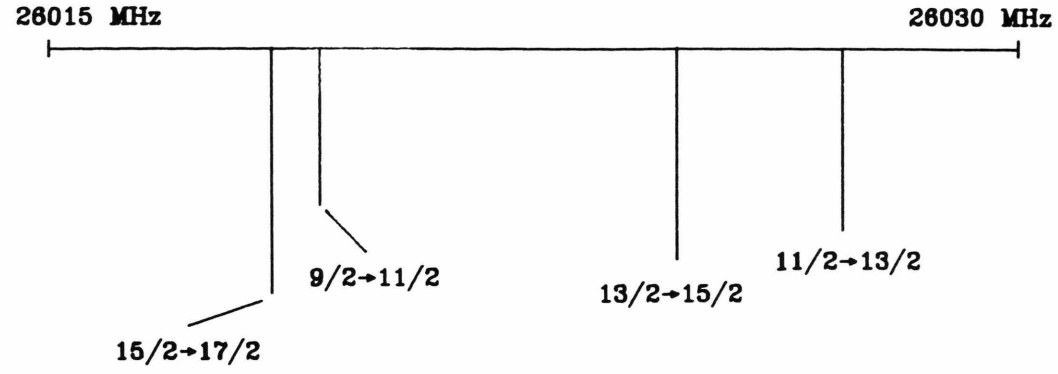

a)

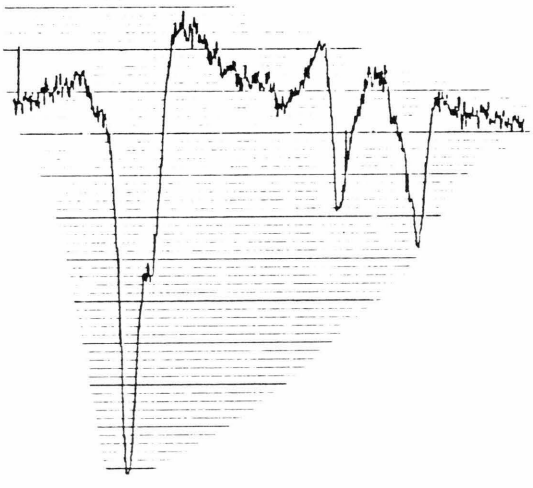

c)

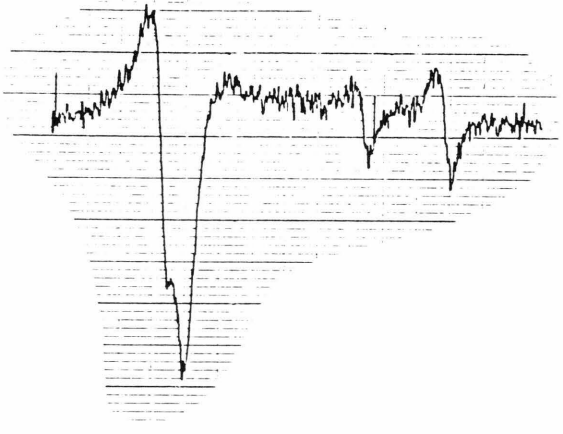

b)

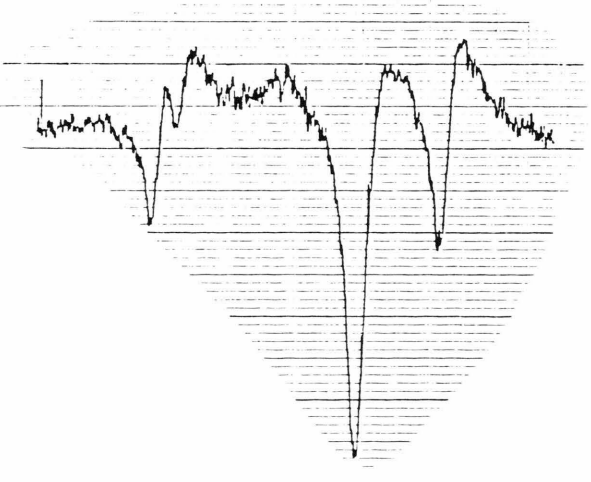

d)

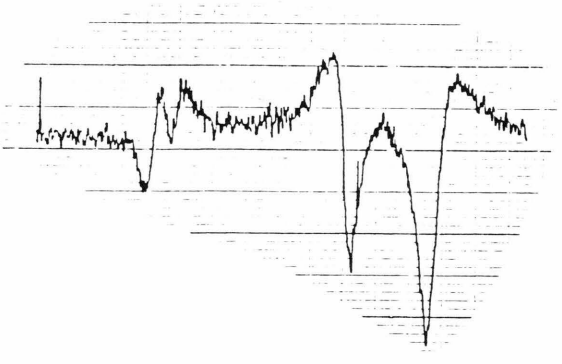

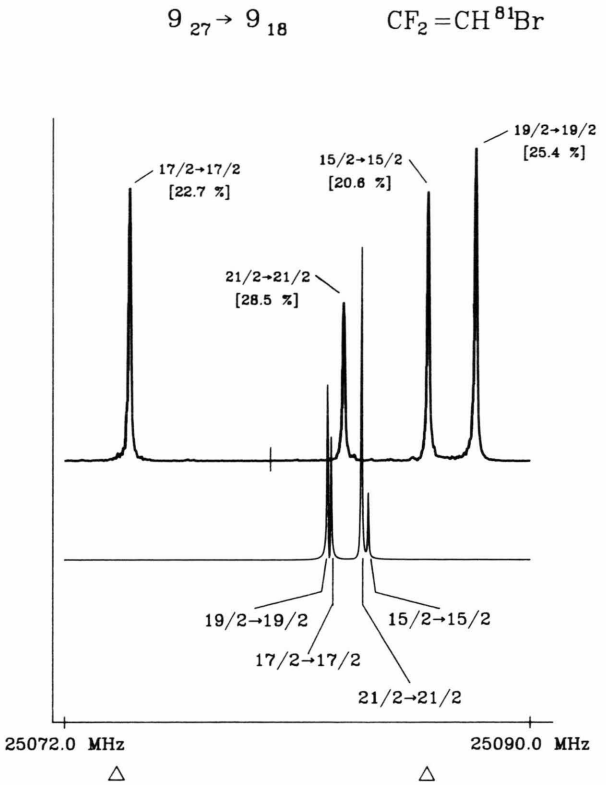

Fig. 5. Some hfs patterns such as the one of the $9_{27} \rightarrow 9_{18}$ rotational transition of $CF_2=CH^{81}Br$ carry direct information on the off-diagonal quadrupole coupling tensor element χ_{ab}. This is caused by accidental close degeneracies of asymmetric top states connected by matrix elements due to χ_{ab} (compare Figure 6). The upper trace shows the experimental spectrum. The lower trace shows a simulation calculated under the neglect of χ_{ab}.

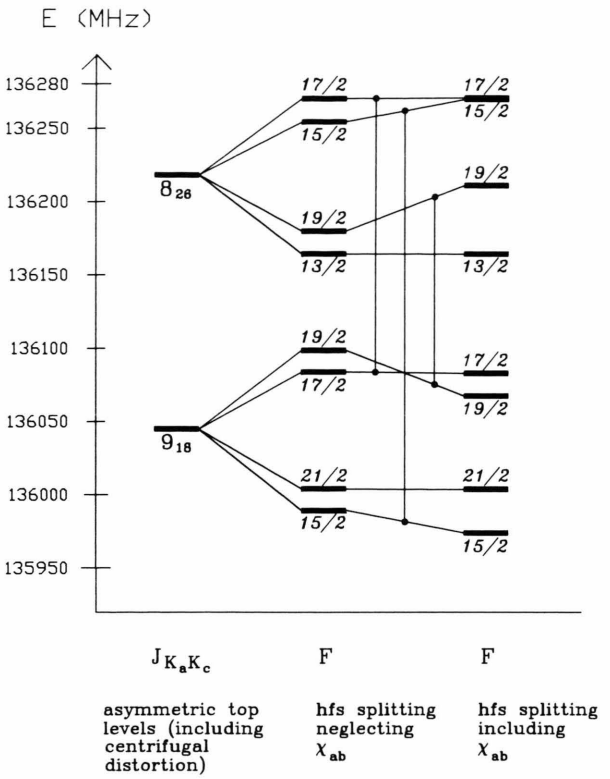

Fig. 6. hfs matrix elements associated with χ_{ab} are off-diagonal in the rotational quantum numbers JK_aK_c. Therefore, in most cases they only lead to minor shifts of the hfs sublevels ($\dashrightarrow$ second order perturbation theory). However, in the case of accidental close degeneracies shown here, these shifts can become substantial. Vertical connections indicate nonvanishing hfs matrix elements associated with χ_{ab}. The 9_{18} state is involved as the lower state in the heavily perturbed hfs pattern shown in Figure 5.

the three quadrupole coupling constants $(\chi_{bb}+\chi_{cc})$, $(\chi_{bb}-\chi_{cc})$, and χ_{ab} were fitted simultaneously.

In view of the sufficiently close "accidental degeneracy" of different rotational states, also χ_{ab} could be determined with high accuracy (comp. Figs. 5 and 6).

In Tables 1 and 2 we present our observed and assigned transition frequencies. In Tables 3 and 4 we present the molecular parameters together with the correlation matrix of the fit.

Discussion

A) Bromine Nuclear Quadrupole Coupling

Sufficiently close accidental degeneracies allowed for an accurate experimental determination of the off-diagonal coupling constants, χ_{ab}. Thus the quadrupole coupling tensors of both isotopic species could be completely determined including their orientation with respect to the molecular principal inertia axes.

Fig. 4. Double resonance spectra corresponding to the MWFT spectrum shown in Figure 3. The hfs pattern of the $7_{16} \rightarrow 7_{25}$ transition does not show up any more since its intensity is not modulated by the pump radiation. The different intensity patterns arise because of different settings of the pump frequency: a) pump at 11 294.70 MHz corresponding to the $F=15/2 \rightarrow F'=15/2$ satellite of the $6_{06} \rightarrow 60_{15}$ transition; b) pump set to 11 299.66 MHz ($9/2 \rightarrow 9/2$ satellite); c) pump set to 11 271.92 MHz ($13/2 \rightarrow 13/2$ satellite); d) pump set to 11 277.30 MHz ($11/2 \rightarrow 11/2$ satellite). The "bar spectrum" gives the relative hfs intensities as they would be observed in a cw-spectrometer.

Table 1. Assigned rotational transitions for the vibronic ground state of $F_2C{=}CH^{79}Br$. Only μ_b-type transitions could be observed. The calculated frequencies were obtained from the molecular parameters presented in Table 3 by numerical diagonalization of the Hamiltonian matrix corresponding to (1). As experimental frequencies we present our microwave Fourier transform results. They were directly fitted to the observed transient emission signals [25].

J'	K'_a	K'_c	→	J	K_a	K_c	F'	F	ν_{exp} [MHz]	ν_{center} [MHz]	$\nu_{calc.}$ [MHz]	$\nu_{exp.-calc.}$ [kHz]
a) μ_b-type-Q-branch-transitions												
2	1	1		2	0	2	5/2	5/2	9 565.617	9 614.587	9 565.621	−3.7
3	1	2		3	0	3	3/2	3/2	9 926.594	9 884.108	9 926.592	1.5
							5/2	5/2	9 867.470		9 867.474	−3.6
							7/2	7/2	9 856.446		9 856.450	−4.4
							9/2	9/2	9 895.238		9 895.237	1.3
3	2	1		3	1	2	3/2	3/2	27 599.490	27 543.336	27 599.500	−9.6
							5/2	5/2	27 537.043		27 537.041	2.2
							7/2	7/2	27 498.935		27 498.921	14.1
							9/2	9/2	27 570.871		27 570.871	0.5
4	1	3		4	0	4	7/2	7/2	10 238.185	10 251.913	10 238.187	−2.2
							9/2	9/2	10 225.654		10.225.660	−6.4
5	1	4		5	0	5	7/2	7/2	10 742.148	10 725.105	10 742.146	2.2
							9/2	9/2	10 713.030		10.713.028	2.1
							11/2	11/2	10 705.544		10 705.546	−2.4
							13/2	13/2	10 735.796		10 735.792	4.3
5	2	3		5	1	4	7/2	7/2	26 854.423	26 840.587	26 854.410	13.4
							9/2	9/2	26 835.958		26 835.959	−1.4
							11/2	11/2	26 828.613		26 828.611	1.7
							13/2	13/2	26 848.972		26 848.978	−5.6
5	2	4		5	1	5	7/2	7/2	29 402.698	29 368.279	29 402.705	−7.4
							9/2	9/2	29 351.482		29.351.495	−12.9
							11/2	11/2	29 337.389		29.337.396	−7.4
							13/2	13/2	29 387.993		29 387.986	7.3
6	1	5		6	0	6	11/2	11/2	11 301.854	11 312.334	11 301.853	0.6
							13/2	13/2	11 295.227		11 295.230	−3.4
							15/2	15/2	11 322.653		11 322.654	−0.4
6	2	4		6	1	5	9/2	9/2	26 418.689	26 411.648	26 418.687	1.9
							11/2	11/2	26 408.553		26.408.551	2.5
							13/2	13/2	26 405.305		26 405.306	−0.5
							15/2	15/2	26 416.956		26 416.946	10.3
6	2	5		6	1	6	11/2	11/2	29 876.293	29 898.785	29 876.296	−2.5
							13/2	13/2	29 874.419		29 874.427	−8.1
							15/2	15/2	29 915.513		29 915.504	9.2
7	1	6		7	0	7	11/2	11/2	12 038.072	12 023.534	12 038.074	−1.8
							13/2	13/2	12 013.045		12 013.046	−0.7
							15/2	15/2	12 007.556		12 007.555	1.3
							17/2	17/2	12 033.754		12 033.751	2.8
7	2	5		7	1	6	11/2	11/2	25 954.963	25 950.941	25 954.961	2.1
							13/2	13/2	25 950.153		25 950.151	2.4
							15/2	15/2	25 947.820		25 947.815	4.9
							17/2	17/2	25 954.765		25 954.775	−10.5
7	2	6		7	1	7	11/2	11/2	30 541.802	30 520.150	30 541.795	6.4
							13/2	13/2	30 506.465		30 506.455	9.9
							15/2	15/2	30 499.794		30 499.787	7.3
							17/2	17/2	30 534.955		30 534.952	2.9
8	2	6		8	1	7	13/2	13/2	25 478.933	25 476.190	25 478.935	−1.7
							15/2	15/2	25 490.639		25 490.638	0.9
							17/2	17/2	25 475.938		25 475.938	0.4
							19/2	19/2	25 509.113		25 509.116	−3.1
8	2	7		8	1	8	13/2	13/2	31 251.957	31 233.223	31 251.956	1.6
							15/2	15/2	31 220.714		31 220.716	−2.6
							17/2	17/2	31.215.488		31 215.494	−6.3
9	1	8		9	0	9	15/2	15/2	13 860.305	13 861.563	13 860.309	−3.8
							21/2	21/2	13 872.044		13 872.042	2.1

Table 1 (continued)

J'	K'_a	K'_c	→	J	K_a	K_c	F'	F	ν_{exp} [MHz]	ν_{center} [MHz]	$\nu_{calc.}$ [MHz]	$\nu_{exp.-calc.}$ [kHz]
9	2	7		9	1	8	15/2	15/2	25 027.357	25 006.890	25 027.358	−0.8
							17/2	17/2	25 009.041		25 009.024	17.8
							19/2	19/2	25 036.945		25 036.962	−17.1
							21/2	21/2	25 006.759		25 006.760	−1.2
9	2	8		9	1	9	15/2	15/2	32 053.889	32 038.785	32 053.897	−7.6
							17/2	17/2	32 024.131		32 024.132	−1.1
							19/2	19/2	32 022.911		32 022.904	6.9
							21/2	21/2	32 051.492		32 051.486	6.2
10	2	8		10	1	9	17/2	17/2	24 562.881	24 563.770	24 562.887	−6.0
							19/2	19/2	24 563.007		24.563.005	2.0
							21/2	21/2	24 561.769		24 561.771	−1.7
							23/2	23/2	24 563.926		24 563.926	−0.5
10	2	9		10	1	10	17/2	17/2	32 953.358	32 937.483	32 953.364	−5.5
							19/2	19/2	32 927.276		32 927.257	19.6
							23/2	23/2	32 949.695		32 949.697	−2.4
11	2	9		11	1	10	19/2	19/2	24 167.905	24 168.154	24 167.912	−6.1
							21/2	21/2	24 167.499		24 167.500	−0.6
							23/2	23/2	24 166.688		24 166.689	−0.5
							25/2	25/2	24 168.479		24 168.481	−2.5
12	2	10		12	1	11	21/2	21/2	23 841.421	23 841.269	23 841.416	5.4
							23/2	23/2	23 840.486		23 840.482	3.8
							25/2	25/2	23 839.708		23 839.710	−1.7
							27/2	27/2	23 841.863		23 841.863	0.1
13	1	12		13	0	13	23/2	23/2	19 499.070	19 484.142	19 499.072	−1.5
							25/2	25/2	19 472.297		19 472.293	3.3
							27/2	27/2	19 469.828		19.469.824	4.3
							29/2	29/2	19 495.811		19 495.808	2.6
13	2	11		13	1	12	23/2	23/2	23 604.136	23 603.604	23 604.138	−1.8
							25/2	25/2	23 602.524		23 602.521	2.2
							27/2	27/2	23 601.660		23 601.658	1.9
							29/2	29/2	23 604.557		23 604.563	−6.1
14	1	13		14	0	14	25/2	25/2	21 348.068	21 333.097	21 348.076	−7.7
							27/2	27/2	21 320.969		21 320.973	−4.4
							29/2	29/2	21 318.611		21 318.613	−1.5
							31/2	31/2	21 345.037		21 345.037	−0.4
14	2	12		14	1	13	25/2	25/2	23 475.248	23 474.393	23 475.254	−6.1
							27/2	27/2	23 472.924		23 472.913	11.6
							29/2	29/2	23 471.794		23 471.798	−4.1
							31/2	31/2	23 475.795		23 475.793	2.1
b) μ_b-type-R-branch-transitions												
3	2	2		2	1	1	5/2	3/2	35 982.299	35 989.137	35 982.309	−10.3
							7/2	5/2	35 959.334		35 959.337	−2.7
							9/2	7/2	35 998.003		35 998.005	−2.6
4	1	4		3	0	3	5/2	3/2	19 432.308	19 416.423	19 432.291	16.8
							7/2	5/2	19 426.550		19 426.536	14.2
							9/2	7/2	19 415.785		19 415.774	11.1
							11/2	9/2	19 413.385		19 413.370	14.9
5	1	5		4	0	4	7/2	5/2	21 721.340	21 727.430	21 721.332	8.1
							9/2	7/2	21 732.566		21 732.559	6.9
							13/2	11/2	21 723.440		21 723.431	8.8
6	1	6		5	0	5	9/2	7/2	23 992.702	23 967.080	23 992.693	9.0
							11/2	9/2	23 980.291		23 980.296	−5.0
							13/2	11/2	23 967.992		23 967.985	7.4
							15/2	13/2	23 962.650		23 962.555	4.5
6	0	6		5	1	5	9/2	7/2	8 206.034	8 199.180	8 206.039	−4.9
							11/2	9/2	8 202.105		8 202.110	−4.7
							13/2	11/2	8 196.734		8 196.736	−1.8
							15/2	13/2	8 198.545		8 198.542	2.7

Table 1 (continued)

J'	K'_a	K'_c	→	J	K_a	K_c	F'	F	ν_{exp} [MHz]	ν_{center} [MHz]	$\nu_{calc.}$ [MHz]	$\nu_{exp.-calc.}$ [kHz]
7	1	7		6	0	6	11/2	9/2	26 139.880	26 143.991	26 139.882	−2.1
							13/2	11/2	26 149.774		26 149.771	2.9
							15/2	13/2	26 146.529		26 146.529	−0.4
							17/2	15/2	26 139.206		26 139.212	−5.2
7	0	7		6	1	6	13/2	11/2	11 331.632	11 338.606	11 331.637	−5.4
							15/2	13/2	11 334.950		11 334.953	−3.2
							17/2	15/2	11 339.363		11 339.362	1.0
8	1	8		7	0	7	13/2	11/2	28 263.705	28 268.448	28 263.708	−2.5
							15/2	13/2	28 273.912		28 273.919	−6.8
							17/2	15/2	28 271.719		28 271.719	0.0
							19/2	17/2	28 263.592		28 263.604	−12.0
8	0	8		7	1	7	15/2	13/2	14 510.131	14 511.039	14 510.136	−5.3
							17/2	15/2	14 506.956		14 506.962	−6.0
9	1	9		8	0	8	15/2	13/2	30 347.141	30 352.147	30 347.133	8.4
							17/2	15/2	30 357.349		30 357.351	−2.4
							19/2	17/2	30 355.674		30 355.672	2.1
							21/2	19/2	30 347.371		30 347.376	−4.9
10	1	10		9	0	9	17/2	15/2	32 402.705	32 407.792	32 402.704	1.5
							19/2	17/2	32 412.699		32 412.703	−4.5
							21/2	19/2	32 411.252		32 411.256	−4.0
							23/2	21/2	32 403.204		32 403.201	2.9
10	0	10		9	1	9	17/2	15/2	20 907.175	20 901.387	20 907.176	−0.5
							19/2	17/2	20 899.656		20 899.651	4.8
							21/2	19/2	20 897.548		20 897.542	6.1
							23/2	21/2	20 903.518		20 903.516	2.3
11	0	11		10	1	10	19/2	17/2	24 097.754	24 092.363	24 097.764	−10.4
							21/2	19/2	24 090.536		24 090.536	−0.4
							23/2	21/2	24 088.938		24 088.933	5.4
							25/2	23/2	24 094.490		24 094.491	−1.1
14	1	13		13	2	12	25/2	23/2	18 651.186	18 645.514	18 651.192	−6.1
							27/2	25/2	18 647.715		18 647.709	5.7
							29/2	27/2	18 641.222		18 641.216	6.4
							31/2	29/2	18 652.100		18 652.100	−0.3

To this end the three equations, which relate the observed coupling constants χ_{aa}, χ_{bb} and χ_{ab} to the principal axes coupling constants $\chi_{\alpha\alpha}$, $\chi_{\beta\beta}$ and to the angle ϑ between the α-axis of the coupling tensor and the a-axis of the moment of inertia tensor were solved for ϑ, $\chi_{\alpha\alpha}$, and $\chi_{\beta\beta}$ (compare Figure 7).

$$\chi_{aa} = \cos^2(a\alpha)\,\chi_{\alpha\alpha} + \cos^2(a\beta)\,\chi_{\beta\beta}$$
$$= \cos^2(\vartheta)\,\chi_{\alpha\alpha} + \sin^2(\vartheta)\,\chi_{\beta\beta}, \quad (3)$$

$$\chi_{bb} = \cos^2(b\alpha)\,\chi_{\alpha\alpha} + \cos^2(b\beta)\,\chi_{\beta\beta}$$
$$= \sin^2(\vartheta)\,\chi_{\alpha\alpha} + \cos^2(\vartheta)\,\chi_{\beta\beta}, \quad (4)$$

$$\chi_{ab} = \cos(a\alpha)\cos(b\alpha)\,\chi_{\alpha\alpha} + \cos(a\beta)\cos(b\beta)\,\chi_{\beta\beta}$$
$$= \sin(\vartheta)\cos(\vartheta)\,(\chi_{\beta\beta} - \chi_{\alpha\alpha}). \quad (5)$$

The combination of (5) with the difference between (4) and (3) leads to the equation for ϑ:

$$\vartheta = (1/2)\arctan\left[\frac{2\chi_{ab}}{\chi_{bb} - \chi_{aa}}\right]. \quad (6)$$

Finally, insertion of ϑ into (3) and (4) leads to $\chi_{\alpha\alpha}$ and $\chi_{\beta\beta}$. Our results are presented in Table 5 and pictorially in Figure 7.

As is seen from Fig. 7, the quadrupole coupling tensor is closely aligned to the C–Br-bond. This feature was expected, since the elements of the quadrupole coupling tensor are closely related to the second derivatives of the intramolecular Coulomb potential caused by the charge distribution outside the nucleus (see above).

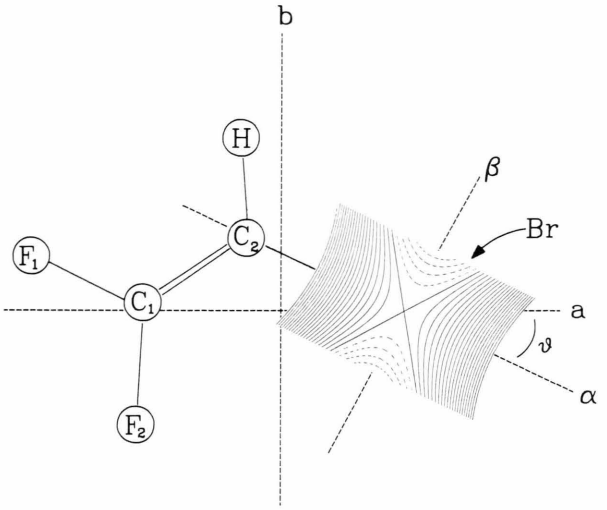

Fig. 7. Assumed structure of $F_2C=CHBr$ with the principal inertia axes a and b and the principal axes α and β of the bromine nuclear quadrupole coupling tensor. The angle ϑ is the angle between the a- and the α-axis. Since χ_{ab} was accessible due to accidental degeneracies it could be determined experimentally with high accuracy. The hyperbolas indicate isopotential curves of the quartic contribution to the intramolecular Coulomb potential which arises from the extranuclear charge distribution. Dashed curves correspond to a negative potential.

It is now interesting to compare the bromine coupling tensors observed here with their values in $H_2C=CHBr$ [11] and $H_3C-HC=CHBr$ [12], which are also given in Table 5 for comparison.

While substitution of hydrogen by the methyl group has only a small effect on the electric field gradient or quadrupole coupling tensor, fluoride substitution causes considerable changes. Within a simplified LCAO-molecular orbital description [13] these changes are directly related to the p-orbital densities (bond order matrix elements), $P_{\alpha\alpha}$, $P_{\beta\beta}$, etc. by

$$\chi_{\alpha\alpha}=h^{-1}eq_{n10}Q\left[P_{\alpha\alpha}-\frac{P_{\beta\beta}+P_{\gamma\gamma}}{2}\right] \text{ (and cyclic permutations).} \quad (7)$$

Here q_{n10} is the expectation value for the second derivative of the Coulomb potential which would be caused by an electron in a valence shell p-orbital of the bromine. With eQq_{n10}/h values from the work of King and Jaccerino [14] (-769.756 MHz for ^{79}Br and -643.033 MHz for ^{81}Br) and with the additional assumption that the in-plane p-orbital perpendicular to the C–Br-bond is doubly occupied, i.e. $P_{\beta\beta}=2$, bromine p-densities were derived from the experimental coupling constants according to (7). They too are presented in Table 5. As is seen from these densities, the main effect of F substitution, at least within the approximations which lead to (7), is to reduce the electron density in the p-orbital in bond direction. This appears intuitively pleasing since the electronegative F-atoms are expected to pull electrons in their direction along the σ-bonds.

For comparison we did also carry out ab initio calculations at the proposed microwave structures, [15, 16] and this work. To this end we did run the Gaussian 88 program of Pople and coworkers [17]. The STO-3G basis was used. The results are also presented in Table 5. For the conversion from the ab initio field gradients (in atomic units) to the quadrupole coupling constants (in MHz) we have used -98.25 MHz/a.u. for ^{79}Br and -78.65 MHz/a.u. for ^{81}Br. These values would correspond to bromine nuclear quadrupole moments of

$$Q^*=0.418\cdot10^{-24}\,\text{cm}^2 \text{ for } ^{79}Br \quad \text{and}$$
$$Q^*=0.335\cdot10^{-24}\,\text{cm}^2 \text{ for } ^{81}Br,$$

respectively. They were fitted for best reproduction of the experimental data and should be regarded as basis set dependent conversion factors rather than the real nuclear quadrupole moments.

For the p-orbitals perpendicular to the C–Br-bond the STO-3G gross p-populations differ from the Townes-Dailey values only by 0.3 to 0.5%. They are systematically lower. The differences of the p-densities in bond direction are slightly larger. Here the STO-3G values are systematically by about 10% lower than the Townes-Dailey results. It appears that the bromine nuclear quadrupole coupling constants can be predicted within about ±2% from STO-3G wavefunctions. The slightly larger discrepancies between the experiment and the STO-3G prediction which are observed in the case of trans-$H_3C-CH=CHBr$ are probably due to the larger experimental uncertainties in the early microwave spectroscopic investigation.

B) Molecular Structure

In principle, microwave spectroscopy provides one of the most accurate methods for the evaluation of molecular structures [18]. This structural information is contained in the rotational constants. Each experimental rotational constant provides one equation of condition which must be fulfilled by the structural parameters. Unfortunately, in planar molecules the

Table 2. Assigned rotational transitions for the vibronic ground state of $F_2C{=}CH^{81}Br$. Only μ_b-type transitions could be observed. The calculated frequencies were obtained from the molecular parameters presented in Table 4 by numerical diagonalization of the Hamiltonian matrix corresponding to (1). As experimental frequencies we present our microwave Fourier transform results. They were directly fitted to the observed transient emission signals [26].

J'	K'_a	K'_c	→	J	K_a	K_c	F'	F	ν_{exp} [MHz]	ν_{center} [MHz]	$\nu_{calc.}$ [MHz]	$\nu_{exp.-calc.}$ [kHz]
μ_b-tpe-Q-branch-transitions												
2	1	1		2	0	2	5/2	5/2	9 580.750	9 622.208	9 580.747	3.0
3	1	2		3	0	3	5/2	5/2	9 873.181	9 886.708	9 873.190	−8.7
							7/2	7/2	9 862.981		9 862.982	−0.7
							9/2	9/2	9 896.214		9 896.217	−2.8
3	2	1		3	1	2	5/2	5/2	27 583.826	27 589.549	27 583.833	−7.1
							9/2	9/2	27 612.279		27 612.277	2.4
4	1	3		4	0	4	5/2	5/2	10 261.832	10 247.507	10 261.829	2.7
							7/2	7/2	10 236.418		10 236.421	−2.9
							9/2	9/2	10 225.818		10 225.810	7.6
							11/2	11/2	10 257.153		10 257.150	2.7
5	1	4		5	0	5	7/2	7/2	10 726.017	10 711.452	10 726.016	0.8
							9/2	9/2	10 701.692		10 701.696	−3.5
							11/2	11/2	10 695.277		10 695.277	−0.2
							13/2	13/2	10 720.450		10 720.449	1.1
5	2	3		5	1	4	7/2	7/2	26 909.344	26 897.937	26 909.346	−1.9
							11/2	11/2	26 887.921		26 887.918	2.9
							13/2	13/2	26 904.820		26 904.821	−0.9
5	2	4		5	1	5	7/2	7/2	29 410.316	29 381.633	29 410.318	−2.4
							9/2	9/2	29 367.571		29 367.578	−6.8
							11/2	11/2	29 355.773		29 355.776	−3.0
							13/2	13/2	29 398.073		29 398.070	2.6
6	1	5		6	0	6	9/2	9/2	11 300.323	11 286.882	11 300.325	−2.4
							11/2	11/2	11 278.246		11 278.246	0.1
							13/2	13/2	11 272.733		11 272.731	1.8
							15/2	15/2	11 295.546		11 295.546	0.0
6	2	4		6	1	5	9/2	9/2	26 480.788	26 474.965	26 480.783	4.3
							11/2	11/2	26 472.240		26 472.239	0.5
							13/2	13/2	26 469.650		26 469.654	−4.0
							15/2	15/2	26 479.246		26 479.238	8.2
6	2	5		6	1	6	9/2	9/2	29 926.947	29 902.421	29 926.954	−7.2
							11/2	11/2	29 897.522		29 897.516	6.0
							13/2	13/2	29 882.022		29 882.024	−1.7
							15/2	15/2	29 916.346		29 916.351	−4.6
7	1	6		7	0	7	11/2	11/2	11 995.696	11 983.397	11 995.698	−1.9
							13/2	13/2	11 974.734		11 974.735	−0.6
							15/2	15/2	11 970.200		11 970.201	−0.7
							17/2	17/2	11 991.955		11 991.957	−2.4
7	2	5		7	1	6	11/2	11/2	26 023.020	26 019.768	26 023.026	−6.2
							13/2	13/2	26 018.870		26 018.867	3.3
							15/2	15/2	26 017.123		26 017.123	−0.1
							17/2	17/2	26 022.709		26 022.705	4.6
7	2	6		7	1	7	13/2	13/2	30 500.941	30 512.369	30 500.935	6.1
							15/2	15/2	30 495.305		30 495.313	−7.6
							17/2	17/2	30 524.691		30 524.687	4.3
8	2	6		8	1	7	13/2	13/2	25 551.526	25 549.452	25 551.529	−2.9
							15/2	15/2	25 553.930		25 553.928	1.9
							17/2	17/2	25 548.691		25 548.689	1.5
							19/2	19/2	25 556.716		25 556.712	3.2
8	2	7		8	1	8	13/2	13/2	31 227.946	31 212.304	31 227.952	−5.8
							15/2	15/2	31 201.860		31 201.861	−0.6
							17/2	17/2	31 197.453		31 197.448	4.9
							19/2	19/2	31 223.555		31 223.550	5.3
9	1	8		9	0	9	15/2	15/2	13 788.642	13 782.048	13 788.632	9.8
							17/2	17/2	13 772.991		13 772.991	0.2
							19/2	19/2	13 764.057		13 764.051	6.0
							21/2	21/2	13 790.800		13 790.805	−5.0
9	2	7		9	1	8	15/2	15/2	25 086.027	25 082.855	25 086.027	0.0
							17/2	17/2	25 074.489		25 074.488	1.3
							19/2	19/2	25 087.882		25 087.889	−7.4
							21/2	21/2	25 082.734		25 082.732	2.3

Table 2 (continued)

J'	K'_a	K'_c	→	J	K_a	K_c	F'	F	ν_{exp} [MHz]	ν_{center} [MHz]	$\nu_{calc.}$ [MHz]	$\nu_{exp.-calc.}$ [kHz]
9	2	8		9	1	9	15/2	15/2	32 016.415	32 002.993	32 016.418	−3.3
							17/2	17/2	31 992.415		31 992.421	−5.9
							19/2	19/2	31 989.678		31 989.675	3.0
10	2	8		10	1	9	17/2	17/2	24 639.354	24 640.057	24 639.359	−4.2
							19/2	19/2	24 639.504		24 639.497	7.4
							21/2	21/2	24 638.555		24 638.546	8.9
							23/2	23/2	24 640.165		24 640.162	2.8
10	2	9		10	1	10	17/2	17/2	32 898.277	32 885.080	32 898.277	−0.1
							19/2	19/2	32 876.418		32 876.416	1.7
							21/2	21/2	32 872.895		32 872.901	−6.3
							23/2	23/2	32 895.164		32 895.160	3.9
b) μ_b-type-R-branch-transitions												
4	1	4		3	0	3	5/2	3/2	19 357.167	19 344.837	19 357.173	−5.5
							7/2	5/2	19 353.137		19 353.139	−1.9
							9/2	7/2	19 343.681		19 343.674	7.3
							11/2	9/2	19 342.282		19 342.274	7.8
5	1	5		4	0	4	7/2	5/2	21 633.814	21 638.308	21 633.808	5.7
							9/2	7/2	21 642.754		21 642.747	6.5
							11/2	9/2	21 635.180		21 635.173	7.2
							13/2	11/2	21 634.964		21 634.952	11.6
6	1	6		5	0	5	9/2	7/2	23 856.327	23 861.407	23 856.330	−2.4
							11/2	9/2	23 858.595		23 858.610	−14.4
							13/2	11/2	23 862.356		23 862.351	4.9
							15/2	13/2	23 857.605		23 857.609	−4.3
7	1	7		6	0	6	11/2	9/2	26 019.155	26 022.436	26 019.164	−8.7
							13/2	11/2	26 027.272		26 027.275	−3.6
							15/2	13/2	26 024.706		26 024.707	−1.0
							17/2	15/2	26 018.425		26 018.423	2.6
7	0	7		6	1	6	11/2	9/2	11 136.921	11 128.892	11 136.916	5.3
							15/2	13/2	11 125.703		11 125.706	−2.6
							17/2	15/2	11 129.534		11 129.536	−1.7
8	1	8		7	0	7	13/2	11/2	28 127.468	28 131.311	28 127.474	−6.4
							15/2	13/2	28 135.900		28 135.895	5.0
							17/2	15/2	28 134.175		28 134.185	−9.7
							19/2	17/2	28 127.242		28 127.240	2.2
8	0	8		7	1	7	13/2	11/2	14 276.895	14 271.621	14 276.903	−7.6
							15/2	13/2	14 270.861		14 270.869	−8.1
							17/2	15/2	14 268.078		14 268.082	−4.4
							19/2	17/2	14 272.930		14 272.935	−5.2
9	1	9		8	0	8	17/2	15/2	30 203.687	30 199.325	30 203.693	−5.8
							19/2	17/2	30 202.415		30 202.416	−1.3
							21/2	19/2	30 195.322		30 195.312	10.1
10	1	10		9	0	9	17/2	15/2	32 234.634	32 238.778	32 234.636	−1.8
							19/2	17/2	32 242.904		32 242.907	−2.6
							21/2	19/2	32 241.835		32 241.835	−0.2
							23/2	21/2	32 234.909		32 234.910	−0.8
10	0	10		9	1	9	17/2	15/2	20 610.056	20 605.280	20 610.060	−4.3
							19/2	17/2	20 603.822		20 603.809	12.6
							21/2	19/2	20 601.932		20 601.921	10.9
							23/2	21/2	20 607.111		20 607.094	16.8
11	0	11		10	1	10	19/2	17/2	23 774.404	23 769.961	23 774.407	−2.4
							21/2	19/2	23 768.402		23 768.406	−3.6
							23/2	21/2	23 766.929		23 766.929	−0.3
							25/2	23/2	23 771.779		23 771.780	−0.3
14	1	13		13	2	12	25/2	23/2	18 128.179	18 123.482	18 128.177	2.2
							27/2	25/2	18 126.932		18 126.932	0.5
							29/2	27/2	18 119.798		18 119.806	−8.0
							31/2	29/2	18 129.615		18 129.611	3.8

Table 3. Vibronic ground state parameters for $F_2C=CH^{79}Br$. They result from the simultaneous fit of the rotational constants, the centrifugal distortion constants and the Br nuclear quadrupole coupling constants to the observed line frequencies listed in Table 1.

A	= 10 717.20898 (90) MHz	D_J	= 0.1729 (8) kHz	
B	= 1 453.47833 (17) MHz	D_{JK}	= 2.262 (7) kHz	
C	= 1 279.25529 (15) MHz	D_K	= 9.56 (19) kHz	
χ_{aa}	= 453.959 (20) MHz	δ_J	= 0.0208 (1) kHz	
$\chi_{bb}-\chi_{cc}$	= 132.662 (9) MHz	R_6	= −0.00333 (8) kHz	
χ_{ab}	= −354.369 (24) MHz			

Correlation matrix:

1.00										
0.17	1.00									
0.04	0.87	1.00								
0.16	0.89	0.89	1.00							
0.29	0.49	0.46	0.63	1.00						
0.81	−0.13	−0.25	−0.19	−0.24	1.00					
0.24	0.22	−0.26	−0.06	−0.06	0.28	1.00				
0.26	0.56	0.48	0.68	−0.72	0.06	0.00	1.00			
0.22	0.00	−0.03	0.00	0.07	0.19	0.05	0.05	1.00		
0.01	0.04	0.05	0.04	0.05	−0.02	−0.01	0.04	0.14	1.00	
0.21	0.13	0.00	0.09	0.00	0.25	0.25	0.07	−0.11	−0.01	1.00

Mean deviation: 6.5 kHz
Number of assigned transitions: 41
Number of hfs-components: 148

Table 4. Vibronic ground state parameters for $F_2C=CH^{81}Br$. They result from the simultaneous fit of the rotational constants, the centrifugal distortion constants and the Br nuclear quadrupole coupling constants to the observed frequencies listed in Table 2.

A	= 10 717.19761 (94) MHz	D_J	= 0.1735 (7) kHz	
B	= 1 439.46581 (15) MHz	D_{JK}	= 2.266 (6) kHz	
C	= 1 268.38766 (14) MHz	D_K	= 9.58 (20) kHz	
χ_{aa}	= 379.262 (24) MHz	δ_J	= 0.0203 (1) kHz	
$\chi_{bb}-\chi_{cc}$	= 110.835 (8) MHz	R_6	= −0.00289 (7) kHz	
χ_{ab}	= −296.094 (34) MHz			

Correlation matrix:

1.00										
0.09	1.00									
−0.02	0.90	1.00								
0.09	0.91	0.90	1.00							
0.25	0.52	0.51	0.66	1.00						
0.83	−0.22	−0.32	−0.26	−0.27	1.00					
0.25	0.16	−0.25	−0.09	−0.10	0.31	1.00				
0.24	0.59	0.52	0.70	0.73	−0.10	−0.02	1.00			
0.03	−0.03	−0.06	−0.04	−0.06	0.07	0.07	−0.03	1.00		
0.05	0.00	−0.01	0.01	0.02	0.03	0.01	0.01	−0.02	1.00	
0.27	0.08	0.01	0.05	−0.14	0.35	0.20	−0.01	0.06	0.04	1.00

Mean deviation: 5.4 kHz
Number of assigned transitions: 39
Number of hfs-components: 144

three equations corresponding to the measured rotational constants are not independent, since they must obey the planarity condition (within the rigid rotor approximation each rotational constant can be calculated from the others by $C^{-1}=A^{-1}+B^{-1}$).

Thus, for planar molecules, each set of three rotational constants, experimentally determined for an individual isotopic species, is equivalent to only two equations of condition for the structural parameters. In our case the situation is even worse, since the heavy bromine atoms are placed almost exactly on the a-axis of the principal inertia axes tensor. This essentially reduces the useful information contained in our measured rotational constants to at most three equations

Table 5. Diagonal elements of the bromine nuclear quadrupole coupling tensors in their own principal axes system (given in MHz) and the corresponding p-orbital densities (or bond order matrix elements) as calculated from (7). The $P_{\beta\beta}$-values were kept fixed to 2.0000 in order to account for the assumption that these electrons do not participate in the chemical bond.

The corresponding STO-3G results are presented in the last two columns. For the conversion from the field gradients to the experimental units we used −98.25 MHz/a.u. and −78.65 MHz/a.u. as conversion factors for ^{79}Br and ^{81}Br, respectively.

The STO-3G p-orbital populations, P_{aa} etc., are the gross orbital populations from the Mulliken population analysis.

	This work		STO-3G	
	$F_2C=CH^{79}Br$	$F_2C=CH^{81}Br$	$F_2C=CH^{79}Br$	$F_2C=CH^{81}Br$
χ_{aa}	615.711(20)	514.425(17)	605.66	484.84
$\chi_{\beta\beta}$	−322.400(14)	−269.376(14)	−314.20	−251.52
$\chi_{\gamma\gamma}$	−293.311(11)	−245.049(13)	−291.46	−233.32
ϑ	−24.534(2)°	−24.536(2)°		
P_{aa}	1.1874	1.1875	1.10240	
$P_{\beta\beta}$	2.0000 (assumed)	2.0000 (assumed)	1.98975	
$P_{\gamma\gamma}$	1.9748	1.9748	1.96900	
	$H_2C=CHBr$			
	^{79}Br [11]	^{81}Br	[^{79}Br]	[STO-3G]	[^{81}Br]
χ_{aa}	543.81	453.61	581.95		465.85
$\chi_{\beta\beta}$	−289.80	−241.44	−307.32		−246.01
$\chi_{\gamma\gamma}$	−254.02	−212.17	−274.63		−219.84
P_{aa}	1.2780	1.2794	1.13332		
$P_{\beta\beta}$	2.0000 (assumed)	2.0000 (assumed)	1.99070		
$P_{\gamma\gamma}$	1.9690	1.9697	1.96189		
	trans-$H_3C-CH=CHBr$				
	^{79}Br [12]	^{81}Br	[^{79}Br]	[STO-3G]	[^{81}Br]
χ_{aa}	557.7	450.3	582.23		466.08
$\chi_{\beta\beta}$	−300.0	−236.8	−305.00		−244.16
$\chi_{\gamma\gamma}$	−257.8	−213.5	−277.23		−221.92
P_{aa}	1.2571	1.2877	1.13584		
$P_{\beta\beta}$	2.0000 (assumed)	2.0000 (assumed)	1.98969		
$P_{\gamma\gamma}$	1.9635	1.9758	1.96476		

of condition, one corresponding to the A constant which is essentially equal for both bromine species, and two corresponding to the two different B constants.

In practice only two structural parameters could be fitted to the observed rotational constants simultaneously.

In view of our interest in approximate values of the rotational constants of the remaining isotopic species we ventured to exploit already this limited structural information for predictive purposes.

Several fits including two free structural parameters were carried out. The results which were most pleasing to us in view of known structural information for

Table 6. Assumed structure for 1-bromo-2,2-difluoroethylene. The bond angles $F_1-C_1=C_2$ and $Br-C_2=C_1$ were fitted to the observed rotational constants for the ^{79}Br-species, $A(^{79}Br)=10.717\,208$ GHz and $B(^{79}Br)=1.453\,478$ GHz, respectively. During this fit the angle $F_2-C_1=C_2$ was kept 1° larger than the angle $F_1-C_1=C_2$ in order to account for "$F_2\cdots Br$ repulsion". All other parameters were kept fixed. The calculated rotational constants presented in Table 7 were obtained from this structure with the fitted angles rounded to four decimals.

Bond distances	
$C_1=C_2$	1.310 Å
C_2-H	1.079 Å
C_1-F_1	1.320 Å
C_1-F_2	1.323 Å
C_2-Br	1.882 Å
Bond angles	
$H-C_2=C_1$	123.5°
$F_1-C_1=C_2$	124.1318° (optimized)
$F_2-C_1=C_2$	125.1318° (set as $F_1-C_1=C_2+1°$)
$Br-C_2=C_1$	121.5132°

Table 7. Calculated rotational constants for

$F_2C=CH^{79}Br$, $F_2C=CH^{81}Br$,
$F_2{}^{13}C=CH^{79}Br$, $F_2C={}^{13}CH^{79}Br$,
$F_2{}^{13}C=CH^{81}Br$, $F_2C={}^{13}CH^{81}Br$.

The values were obtained within the rigid rotor approximation from the structure presented in Table 6. For the prediction of the ^{13}C spectra, the calculated C constants should be reduced by about 640 kHz in order to account for the inertial defect. From fits with other sets of present values we expect the predicted ^{13}C rotational constants to be accurate within ±5 MHz (our predictions did fall into a range of only ±1 MHz). Note how well all six experimental rotational constants are reproduced from the assumed structure even though only $A(^{79}Br)$ and $B(^{81}Br)$ were used in the fit of the bond angles.

Rotat. const.	$F_2C=CH^{79}Br$	$F_2{}^{13}C=CH^{79}Br$	$F_2C={}^{13}CH^{79}Br$
A	10.717208 GHz	10.715761 GHz	10.574276 GHz
B	1.453478 GHz	1.444322 GHz	1.452835 GHz
C	1.279898 GHz	1.272772 GHz	1.277337 GHz
	$F_2C=CH^{81}Br$	$F_2{}^{13}C=CH^{81}Br$	$F_2C={}^{13}CH^{81}Br$
A	10.717208 GHz	10.715761 GHz	10.574268 GHz
B	1.439469 GHz	1.430267 GHz	1.438777 GHz
C	1.269022 GHz	1.261844 GHz	1.266458 GHz

related molecules [19–22] are presented in Tables 6 and 7. To derive this structure we kept all bond lengths fixed to values slightly shorter than reported for related molecules. This was done in order to account for the shrinking in adjacent bonds, which is typical for the substitution of hydrogen atoms by halogen atoms [23].

The H–C=C bond angle was kept fixed to 123.5° i.e. about the value in $F_2C=CHCl$ [24] (all rotational constants depend very little on its exact value). The $F_2–C_1=C_2$ angle, where F_2 is the fluorine cis to bromine, was set as 1° larger than the $F_1–C_1–C_2$ angle in order to account for F···Br repulsion, and finally the angles $F_1–C_1=C_2$ and $Br–C_2=C_1$ were fitted to the experimental rotational constants *A* and *B* for the ^{79}Br species. Essentially the same procedure was carried out with $\measuredangle F_1–C_1=C_2 = \measuredangle F_2–C_1=C_2$ and with $\measuredangle F_1–C_1=C_2 = \measuredangle F_2–C_1=C_2 + 2°$, but our proposed structure obtained for the 1° difference is slightly better in reproducing all six observed rotational constants. Further fits with slightly increased bond lengths were also carried out in order to get some feeling for the uncertainties in the rotational constants predicted for the monosubstituted ^{13}C-species.

In all these fits the predicted ^{13}C rotational constants varied only within a range of ±1 MHz. Therefore, if we include an additional uncertainty of ±4 MHz to account for differences in the effects of zero point vibrations, we believe that a total uncertainty in the rotational constants of ±5 MHz will provide reasonable bounds for searching the hitherto unassigned ^{13}C transitions.

With the dramatic increase in sensitivity gained by the combination of microwave Fourier transform spectroscopy and molecular beam techniques, such a search should be feasible even with ^{13}C species in natural abundance. It is planned at our laboratory in the near future.

Acknowledgement

We are glad to acknowledge financial support by Deutsche Forschungsgemeinschaft. Dr. H. Krause kindly carried out the ab initio calculations. We are also grateful for free computer time, granted by the computer center of the University Kiel.

We would like to thank Prof. Dr. A. Guarnieri for critically reading the manuscript.

[1] V. W. Laurie and D. T. Pence, J. Chem. Phys. **38,** 2693 (1962).
[2] D. de Kerckhove Varent, Ann. Soc. Sci. Bruxelles **84,** 277 (1970).
[3] H. D. Rudolph, Z. Angew. Phys. **13,** 401 (1961).
[4] R. P. Blickensderfer, J. H. S. Wang, and W. H. Flygare, J. Chem. Phys. **51,** 3196 (1969).
[5] P. Kisliuk and C. H. Townes, Nat. Bur. Stand. Circ. **1952,** 518.
[6] B. P. van Eijck, J. Mol. Spectr. **53,** 246 (1974).
[7] V. Typke, J. Mol. Spectr. **63,** 170 (1976).
[8] W. Gordy and R. L. Cook, Microwave Molecular Spectra, Chapt. IX, 3rd ed., John Wiley and Sons, New York 1984.
[9] H. P. Benz, A. Bauder, and H. H. Günthard, J. Mol. Spectr. **21,** 156 (1966).
[10] Author: J. Gripp, Dissertation, Kiel 1989.
[11] Loc. cit. [2].
[12] R. A. Beaudet, J. Chem. Phys. **50,** 2002 (1969).
[13] J. Mjöberg and S. Ljungren, Z. Naturforsch. **28a,** 729 (1973).
[14] J. G. King and V. Jaccerino, Phys. Rev. **94,** 1610 (1954).
[15] Loc. cit. [2].
[16] Loc. cit. [12].
[17] Gaussian 88, M. J. Frisch, M. Head-Gordon, H. B. Schlegel, K. Raghavachari, J. S. Binkley, C. Gonzalez, D. J. Defrees, D. J. Fox, R. A. Whiteside, R. Seeger, C. F. Melius, J. Baker, R. L. Martin, L. R. Kahn, J. J. P. Stewart, E. M. Fluder, E. S. Topiol, and J. A. Pople, Gaussian, Inc., Pittsburgh PA. 1988.
[18] Loc. cit. [8], Chapt. XIII.
[19] Loc. cit. [1].
[20] R. G. Stone and W. H. Flygare, J. Chem. Phys., **49,** 1943 (1968).
[21] R. G. Stone and W. H. Flygare, J. Mol. Spectr. **32,** 233 (1969).
[22] Loc. cit. [2].
[23] H. A. Bent, J. Chem. Phys. **33,** 1258 (1960).
[24] Loc. cit. [20].
[25] J. Haekel and H. Mäder, Z. Naturforsch. **43a,** 203 (1988).
[26] Loc. cit. [25].